J|A|C|S
ARTICLES

Published on Web 12/09/2008

Observation of a Low-Temperature, Dynamically Driven Structural Transition in a Polypeptide by Solid-State NMR Spectroscopy

Vikram S. Bajaj,[†] Patrick C.A. van der Wel,[‡] and Robert G. Griffin*

Francis Bitter Magnet Laboratory and Department of Chemistry, Massachusetts Institute of Technology, Cambridge, Massachusetts 02139

Received June 21, 2008; E-mail: rgg@mit.edu

Abstract: At reduced temperatures, proteins and other biomolecules are generally found to exhibit dynamic as well as structural transitions. This includes a so-called protein glass transition that is universally observed in systems cooled between 200 and 230 K, and which is generally attributed to interactions between hydrating solvent molecules and protein side chains. However, there is also experimental and theoretical evidence for a low-temperature transition in the intrinsic dynamics of the protein itself, absent any solvent. Here, we use low-temperature solid-state NMR to examine site-specific fluctuations in atomic structure and dynamics in the absence of solvents. In particular, we employ magic angle spinning NMR to examine a structural phase transition associated with dynamic processes in a solvent-free polypeptide, N-*f*-MLF-OH, lattice at temperatures as low as 90 K. This transition is characterized by the appearance of an extra set of lines in 1D ^{15}N spectra as well as additional cross peaks in 2D ^{13}C−^{13}C and ^{13}C−^{15}N spectra. Interestingly, the gradual, temperature-dependent appearance of the new spectral component is not accompanied by the line broadening typical of dynamic transitions. A direct comparison between the spectra of N-*f*-MLF-OH and the analog N-*f*-MLF-OMe, which does not display this transition, indicates a correlation of the structural transition to the temperature dependent motion of the aromatic phenylalanine side chain. Several quantitative solid state NMR experiments were employed to provide site-specific measurements of structural and motional features of the observed transition.

Introduction

The role of dynamics and flexibility in protein function has been clear since the very first crystal structure.[1] To bind substrate or channel a chemical reaction forward, an enzyme assumes one or more conformational states in sequence, such that energy is transduced in the desired direction. Transitions between these local energy minima, which are near the global minimum of the protein energy landscape, are mediated by concerted dynamical rearrangements at ambient temperatures.[2−4] At the same time, a protein must be sufficiently robust and stable to reliably adopt a unique conformation or set of conformations that are essential for its function. This balance between conformational flexibility and structural robustness has evolved in each protein to allow it to function in its native environment. This has been experimentally observed as a temperature-dependent loss or gain of activity for various biological systems that correlates to specific changes in protein flexibility.[5−7] This is true not only for globular proteins, but also for membrane protein−lipid complexes such as photosystem II[8] and bacteriorhodopsin.[9] Interestingly, the temperature at which this loss of dynamics and function occurs appears largely independent of the type of system. This seemingly universal transition occurs at 200−230 K, and is known as the "protein dynamical transition" or the "protein glass transition".[10−15] The latter name relates to the observed analogy with the dynamics encountered in disordered media such as liquids. A similar transition has even been observed in other biological macromolecules.[16]

[†] Present address: Lawrence Berkeley National Laboratory and University of California, Berkeley, CA 94720.

[‡] Present address: Department of Structural Biology, University of Pittsburgh School of Medicine, Pittsburgh, PA 15260.

(1) Kendrew, J. C.; Bodo, G.; Dintzis, H. M.; Parrish, R. G.; Wyckoff, H.; Phillips, D. C. *Nature* **1958**, *181* (4610), 662–666.
(2) Elber, R.; Karplus, M. *Science* **1987**, *235* (4786), 318–321.
(3) Elber, R.; Karplus, M. *Phys. Rev. Lett.* **1986**, *56* (4), 394–397.
(4) Kushida, T.; Ahn, J. S.; Hirata, K.; Kurita, A. *Biochem. Biophys. Res. Commun.* **1989**, *160* (2), 948–53.
(5) Rasmussen, B. F.; Stock, A. M.; Ringe, D.; Petsko, G. A. *Nature* **1992**, *357* (6377), 423–424.
(6) Lichtenegger, H.; Doster, W.; Kleinert, T.; Birk, A.; Sepiol, B.; Vogl, G. *Biophys. J.* **1999**, *76* (1), 414–422.
(7) Ding, X. C.; Rasmussen, B. F.; Petsko, G. A.; Ringe, D. *Bioorg. Chem.* **2006**, *34* (6), 410–423.
(8) Pieper, J.; Irrgang, K. D.; Ratsep, M.; Voigt, J.; Renger, G.; Small, G. J. *Photochem. Photobiol.* **2000**, *71* (5), 574–581.
(9) Lechner, R. E.; Fitter, J.; Dencher, N. A.; Hau, T. *Phys. B: Condens. Matter* **2006**, *385−386*, 835–837.
(10) Iben, I. E. T.; Braunstein, D.; Doster, W.; Frauenfelder, H.; Hong, M. K.; Johnson, J. B.; Luck, S.; Ormos, P.; Schulte, A.; Steinbach, P. J.; Xie, A. H.; Young, R. D. *Phys. Rev. Lett.* **1989**, *62* (16), 1916.
(11) Ringe, D.; Petsko, G. A. *Biophys. Chem.* **2003**, *105*, 667–680.
(12) Vitkup, D.; Ringe, D.; Petsko, G. A.; Karplus, M. *Nat. Struct. Biol.* **2000**, *7* (1), 34–38.
(13) Lee, A. L.; Wand, A. J. *Nature* **2001**, *411* (6836), 501–504.
(14) Gutin, A.; Sali, A.; Abkevich, V.; Karplus, M.; Shakhnovich, E. I. *J. Chem. Phys.* **1998**, *108* (15), 6466–6483.
(15) Mok, K. H.; Nagashima, T.; Day, I. J.; Jones, J. A.; Jones, C. J. V.; Dobson, C. M.; Hore, P. J. *J. Am. Chem. Soc.* **2003**, *125* (41), 12484–12492.

10.1021/ja8045926 CCC: $40.75

There have been a number of studies that have attempted to characterize the physical basis of this process. Experimental data from X-ray crystallography[17,18] and FTIR[19] and molecular dynamics simulations[12] support the idea that the protein glass transition is due to a coupling of the protein motions with the dynamics of the solvent. The dynamic modes of the bulk water molecules, in particular, appear to influence the motion of the polypeptide chain; ordering of water at low temperatures is then associated with a loss of this dynamically driven activation[17] through a solvent caging effect. At temperatures slightly above the glass transition, ordering of bound waters results in increased local viscosity and prevents the anharmonic and concerted protein motions that give rise to mechanistically significant rearrangements. This has been supported by studies showing that the transition temperature can be modulated by changes in the viscosity of the solvent system.[20−22]

Aside from these solvent-dependent contributions to the protein glass transition,[13,16,22−24] more recent data have highlighted residual anharmonic motions occurring below 200 K and showed that these motions appear independent of the hydration state. This solvent independence has been observed in neutron scattering experiments on dehydrated myoglobin,[25] lysozyme[16,26] and photosystem II,[24] molecular dynamics simulations in the absence of solvent,[27] and the extrapolated results of solution-state NMR experiments at ambient temperatures.[13] Recent molecular dynamics simulations by Vitkup and coworkers[12] suggest that solvent mobility dominates the glass transition down to 180 K, and that intrinsic protein dynamics play the dominant role at lower temperatures. Therefore, the onset of anharmonic motions near 100 K appears to be an intrinsic property of the protein conformational energy surface alone. It was suggested that these dynamics are dominated by the onset of thermally activated methyl group rotations.[13,16,23] Interestingly, previous solid-state ^{2}H NMR studies of $-CH_3$ group motion in Val and Ala have shown that thermally activated 3-fold hops initiate at 110 and 133 K, respectively.[28,29]

Clearly, the low-temperature dynamic behavior of proteins is more complex than was initially assumed and a detailed understanding is important for several reasons. First, it will provide insight into the concerted dynamic rearrangements that are necessary for optimal biological function. Second, from a practical perspective, a number of biophysical techniques, including X-ray crystallography, solid-state NMR (SSNMR) and cryo-electron microscopy, frequently require cooling of the sample to temperatures below the protein glass transition temperature. Because the protein in this state is not biologically active, it is important to understand how measured structural parameters change as a function of temperature. Finally, the low temperature dynamics, if better understood, may allow for trapping of mechanistically relevant conformational intermediates.[7,11]

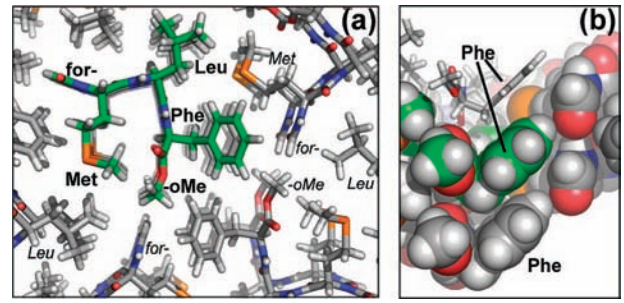

Figure 1. Structure of N-*f*-MLF-OMe crystal lattice.[30] Panel (a) shows a "top-down" view of the crystal lattice. Panel (b) shows the steric crowding and relative orientation of the phenylalanine side chains, allowing aromatic $\pi-\pi$ stacking interactions. This figure was prepared using PyMOL.[31]

Here, we demonstrate the utility of high-resolution, temperature-dependent magic angle spinning (MAS) NMR spectroscopy in a study of the intrinsic dynamics and structure of the chemotactic tripeptide, N-*f*-MLF-OH in the absence of solvent. These tripeptide crystals form a model system for SSNMR experiments and have been well-characterized in previous experiments,[32−35] resulting in an early solid-state NMR-based structure.[36] In the current context, the system is particularly appropriate because it crystallizes in solvent-free microcrystals and yet experiences a representative range of dynamic phenomena. Indeed, a variety of conformational dynamics are known to be present in the lattice, including rotamer interconversion, librational motion of side chains, phenylalanine ring flips, and 3-fold "hopping" of methyl groups, representing a variety of amino acid dynamics observed in proteins in general. Further, the addition of a single methyl group produces N-*f*-MLF-OMe, which adopts a similar crystal structure (Figure 1), as reflected by its similar chemical shifts and powder diffraction patterns. In addition, and in contrast to N-*f*-MLF-OH, the crystal structure of N-*f*-MLF-OMe was solved by X-ray crystallography.[30] However, the latter peptide has one salient structural difference in that its Phe aromatic ring is sterically restricted and thus hindered from flipping. Therefore, in the ^{13}C MAS spectrum of N-*f*-MLF-OMe recorded at 300 K, we observe all six lines from the ring, whereas in N-*f*-MLF-OH, we see lines only from the C_γ and C_ζ ^{13}C's. The lines from C_ε and C_δ are

(16) Caliskan, G.; Briber, R. M.; Thirumalai, D.; Garcia-Sakai, V.; Woodson, S. A.; Sokolov, A. P. *J. Am. Chem. Soc.* **2006**, *128* (1), 32–33.
(17) Teeter, M. M.; Yamano, A.; Stec, B.; Mohanty, U. *Proc. Natl. Acad. Sci. U.S.A.* **2001**, *98* (20), 11242–11247.
(18) Rassmussen, B. F.; Stock, A. M.; Ringe, D.; Petsko, G. A. *Nature* **1992**, *357*, 423–424.
(19) Mayer, E. *Biophys. J.* **1994**, *67* (2), 862–873.
(20) Cordone, L.; Ferrand, M.; Vitrano, E.; Zaccai, G. *Biophys. J.* **1999**, *76* (2), 1043–1047.
(21) Tsai, A. M.; Neumann, D. A.; Bell, L. N. *Biophys. J.* **2000**, *79* (5), 2728–2732.
(22) Cornicchi, E.; Marconi, M.; Onori, G.; Paciaroni, A. *Biophys. J.* **2006**, *91* (1), 289–297.
(23) Roh, J. H.; Novikov, V. N.; Gregory, R. B.; Curtis, J. E.; Chowdhuri, Z.; Sokolov, A. P. *Phys. Rev. Lett.* **2005**, *95* (3), 038101−4.
(24) Pieper, J.; Hauss, T.; Buchsteiner, A.; Baczynski, K.; Adamiak, K.; Lechner, R. E.; Renger, G. *Biochemistry* **2007**, *46* (40), 11398–11409.
(25) Doster, W.; Bachleitner, A.; Dunau, R.; Hiebl, M.; Luscher, E. *Biophys. J.* **1986**, *50* (2), 213–219.
(26) Boswell, P. G.; Lugert, E. C.; Rabai, J.; Amin, E. A.; Buhlmann, P. *J. Am. Chem. Soc.* **2005**, *127* (48), 16976–16984.
(27) Smith, J.; Kuczera, K.; Karplus, M. *Proc. Natl. Acad. Sci. U.S.A.* **1990**, *87* (4), 1601–1605.
(28) Beshah, K.; Olejniczak, E. T.; Griffin, R. G. *J. Chem. Phys.* **1987**, *86* (9), 4730–4736.
(29) Beshah, K.; Griffin, R. G. *J. Magn. Reson.* **1989**, *84* (2), 268–274.
(30) Gavuzzo, E.; Mazza, F.; Pochetti, G.; Scatturin, A. *Int. J. Peptide Protein Res.* **1989**, *34*, 409–415.
(31) DeLano, W. L. *The PyMOL Molecular Graphics System*; DeLano Scientific: Palo Alto, CA, 2002.
(32) Hong, M.; Griffin, R. G. *J. Am. Chem. Soc.* **1998**, *120* (28), 7113–7114.
(33) Ladizhansky, V.; Veshtort, M.; Griffin, R. G. *J. Magn. Reson.* **2002**, *154* (2), 317–324.
(34) Jaroniec, C. P.; Tounge, B. A.; Herzfeld, J.; Griffin, R. G. *J. Am. Chem. Soc.* **2001**, *123* (15), 3507–3519.
(35) Sun, B. Q.; Rienstra, C. M.; Costa, P. R.; Williamson, J. R.; Griffin, R. G. *J. Am. Chem. Soc.* **1997**, *119*, 8540–8546.
(36) Rienstra, C. M.; Tucker-Kellogg, L.; Jaroniec, C. P.; Hohwy, M.; Reif, B.; McMahon, M. T.; Tidor, B.; Lozano-Perez, T.; Griffin, R. G. *Proc. Natl. Acad. Sci. U.S.A.* **2002**, *99*, 10260–10265.

attenuated because of the flipping motion interfering with the $^1H-^{13}C$ decoupling.[37,38]

Solid-state NMR is a robust method of ab initio structure determination that can concurrently provide detailed information about motional processes over a wide range of time scales. Furthermore, there has been significant progress in the development of low-temperature MAS instrumentation in recent years, facilitating an investigation of the protein glass transition.[39,40] In 1D spectra collected as a function of temperature, the effects of dynamics are readily observed. They include classical conformational exchange and interference phenomena that are manifest when dynamic processes occur at rates similar to the magic angle spinning or ^1H decoupling. The tripeptide N-*f*-MLF-OMe provides a rigid reference structure, showing little effect of cooling to temperatures as low as 90 K. In contrast, similar cooling causes dramatic changes in the NMR spectra of the N-*f*-MLF-OH crystals. These changes include the emergence of a structurally distinct substate of the peptide near the glass transition temperature, which we show is correlated to an unusual dynamically driven structural transition occurring between ~90 and ~200 K. The distinct structural forms of the peptide were also characterized using solid state NMR methods previously applied to N-*f*-MLF-OH at room temperature[36] and, more recently, in amyloid fibrils from transthyretin.[41] This strategy involves the application of dipolar recoupling experiments in uniformly labeled systems to measure heteronuclear $^{13}C-^{15}N$ distances[34,42,43] and tensor correlation experiments[33,44−52] to constrain backbone torsion angles. On the basis of our experimental data, we report on the change of dynamics and the correlated changes in structure. The observed dynamic/structural transition is also discussed in terms of its possible relation to the physical origins of intrinsic low temperature protein motions near the protein glass transition.

Methods

Sample Preparation. Unlabeled tripeptides *N-formyl*-Met-Leu-Phe-OH (N-*f*-MLF-OH) and *N-formyl*-Met-Leu-Phe-OCH_3 (N-*f*-MLF-OMe) were obtained from Bachem (King of Prussia, PA). Selectively deuterated N-*f*-MLF-OH containing ring-deuterated Phe-d_5 was prepared by solid-phase peptide synthesis by SynPep Corporation (Dublin, CA). Uniformly labeled *N-f*-[U−^{13}C,U−^{15}N]-MLF-OH was synthesized by solid phase peptide synthesis by CS Bio Inc. (Menlo Park, CA). Isotopically labeled Phe-d_5, FMOC-[U−^{13}C,^{15}N-Met], FMOC-[U−^{13}C,^{15}N-Leu], and FMOC-[U−^{13}C,^{15}N-Phe] were obtained from Cambridge Isotope Laboratories (Andover, MA). N-*f*-MLF-OH and N-*f*-MLF-OMe were crystallized from isopropanol and benzene, respectively, in accordance with previously published protocols.[30,53] Small, needlelike crystals were obtained after dissolution in warm solvent followed by slow evaporation to dryness. Distance and torsion angle measurements were conducted in a sample diluted to 10% in natural abundance peptide prior to crystallization in order to minimize the effects of intermolecular dipolar couplings.

NMR Measurements and Analysis. Magic angle spinning experiments were performed using a home-built spectrometer operating at 380 MHz ^1H frequency (designed by D. J. Ruben, Francis Bitter Magnet Laboratory, MIT) and a triple channel (^1H, ^{13}C, ^{15}N) 4 mm MAS probe designed for low temperature dynamic nuclear polarization (DNP) experiments.[39] Sample cooling was performed by using precooled nitrogen gas to provide the drive and bearing pressure for MAS. The spinning frequency of 6.25−7 kHz was controlled by a Bruker MAS controller (Billerica, MA). At each temperature, ^{13}C chemical shifts were referenced relative to dilute, aqueous DSS using external referencing via the ^{13}C chemical shifts of adamantane,[54] and ^{15}N chemical shifts were referenced indirectly to liquid ammonia using the suggested IUPAC frequency ratios ($^{13}C/^1H$) of aqueous DSS and liquid NH_3 ($^{15}N/^1H$).[55,56] Spectra were processed and visualized using the NMRPipe,[57] Sparky,[58] and CCPNMR [59−62] software packages.

Static deuterium NMR spectra were obtained on a home-built spectrometer operating at 61 MHz ^2H frequency, using a quadrupolar echo pulse sequence[63] with 2 μs $\pi/2$ pulses, a 35 μs echo delay, and a 8−12 s recycle delay. The experimental lineshapes were simulated with an updated version of the ^2H line shape package

(37) Long, J. R.; Sun, B. Q.; Bowen, A.; Griffin, R. G. *J. Am. Chem. Soc.* **1994**, *116*, 11950–11956.
(38) Maus, D. C.; Copie, V.; Sun, B. Q.; Griffiths, J. M.; Griffin, R. G.; Luo, S. F.; Schrock, R. R.; Liu, A. H.; Seidel, S. W.; Davis, W. M.; Grohmann, A. *J. Am. Chem. Soc.* **1996**, *118* (24), 5665–5671.
(39) Bajaj, V. S.; Farrar, C. T.; Hornstein, M. K.; Mastovsky, I.; Vieregg, J.; Bryant, J.; Elena, B.; Kreischer, K. E.; Temkin, R. J.; Griffin, R. G. *J. Magn. Reson.* **2003**, *160*, 85–90.
(40) Bajaj, V. S.; Hornstein, M. K.; Kreischer, K. E.; Sirigiri, J. R.; Woskov, P. P.; Mak-Jurkauskas, M. L.; Herzfeld, J.; Temkin, R. J.; Griffin, R. G. *J. Magn. Reson.* **2007**, *189* (2), 251–279.
(41) Jaroniec, C. P.; MacPhee, C. E.; Bajaj, V. S.; McMahon, M. T.; Dobson, C. M.; Griffin, R. G. *Proc. Natl. Acad. Sci. U.S.A.* **2004**, *101* (3), 711–716.
(42) Gullion, T.; Schaefer, J. *J. Magn. Reson.* **1989**, *81*, 196–200.
(43) Jaroniec, C. P.; Filip, C.; Griffin, R. G. *J. Am. Chem. Soc.* **2002**, *124* (36), 10728–10742.
(44) Hong, M.; Gross, J. D.; Griffin, R. G. *J. Phys. Chem. B* **1997**, *101* (30), 5869–5874.
(45) Reif, B.; Hohwy, M.; Jaroniec, C. P.; Rienstra, C. M.; Griffin, R. G. *J. Magn. Reson.* **2000**, *145* (1), 132–141.
(46) Feng, X.; Eden, M.; Brinkmann, A.; Luthman, H.; Eriksson, L.; Gräslund, A.; Antzutkin, O. N.; Levitt, M. H. *J. Am. Chem. Soc.* **1997**, *119*, 12006–12007.
(47) Feng, X.; Lee, Y. K.; Sandström, D.; Eden, M.; Maisel, H.; Sebald, A.; Levitt, M. H. *Chem. Phys. Lett.* **1996**, *257*, 314–320.
(48) Hohwy, M.; Rienstra, C. M.; Griffin, R. G. *J. Chem. Phys.* **2002**, *117*, 4973–4987.
(49) Hong, M.; Gross, J. D.; Hu, W.; Griffin, R. G. *J. Magn. Reson.* **1998**, *135* (1), 169–177.
(50) Hong, M.; Gross, J. D.; Rienstra, C. M.; Griffin, R. G.; Kumashiro, K. K.; Schmidt-Rohr, K. *J. Magn. Reson.* **1997**, *129*, 85–92.
(51) Ladizhansky, V.; Jaroniec, C. P.; Diehl, A.; Oschkinat, H.; Griffin, R. G. *J. Am. Chem. Soc.* **2003**, *125*, 6827–6833.
(52) Rienstra, C. M.; Hohwy, M.; Mueller, L. J.; Jaroniec, C. P.; Reif, B.; Griffin, R. G. *J. Am. Chem. Soc.* **2002**, *124*, 11908–11922.
(53) Rienstra, C. M.; Hohwy, M.; Hong, M.; Griffin, R. G. *J. Am. Chem. Soc.* **2000**, *122*, 10979–10990.
(54) Morcombe, C. R.; Zilm, K. W. *J. Magn. Reson.* **2003**, *162* (2), 479–486.
(55) Markley, J. L.; Bax, A.; Arata, Y.; Hilbers, C. W.; Kaptein, R.; Sykes, B. D.; Wright, P. E.; Wüthrich, K. *Pure Appl. Chem.* **1998**, *70*, 117–142.
(56) Harris, R. K.; Becker, E. D.; Cabrel de Menezes, S. M.; Goodfellow, R.; Granger, P. *Solid State Nuc. Mag. Reson.* **2002**, *22*, 458−483.
(57) Delaglio, F.; Grzesiek, S.; Vuister, G. W.; Pfeifer, J.; Bax, A. *J. Biomol. NMR* **1995**, *6*, 277–293, NMR PIPE.
(58) Goddard, T. D.; Kneller, D. G. *SPARKY−NMR Assignment Program*; University of California: San Francisco, 2006; available from http://www.cgl.ucsf.edu/home/sparky/.
(59) Fogh, R. H.; Vranken, W. F.; Boucher, W.; Stevens, T. J.; Laue, E. D. *J. Biomol. NMR* **2006**, *36* (3), 147–155.
(60) Vranken, W. F.; Boucher, W.; Stevens, T. J.; Fogh, R. H.; Pajon, A.; Llinas, P.; Ulrich, E. L.; Markley, J. L.; Ionides, J.; Laue, E. D. *Proteins: Struct., Funct, Bioinf,* **2005**, *59* (4), 687–696.
(61) Fogh, R. H.; Boucher, W.; Vranken, W. F.; Pajon, A.; Stevens, T. J.; Bhat, T. N.; Westbrook, J.; Ionides, J. M. C.; Laue, E. D. *Bioinformatics* **2005**, *21* (8), 1678–1684.
(62) Pajon, A.; Ionides, J.; Diprose, J.; Fillon, J.; Fogh, R.; Ashton, A. W.; Berman, H.; Boucher, W.; Cygler, M.; Deleury, E.; Esnouf, R.; Janin, J.; Kim, R.; Krimm, I.; Lawson, C. L.; Oeuillet, E.; Poupon, A.; Raymond, S.; Stevens, T.; van Tilbeurgh, H.; Westbrook, J.; Wood, P.; Ulrich, E.; Vranken, W.; Li, X. L.; Laue, E.; Stuart, D. I.; Henrick, K. *Proteins: Struct., Funct., Bioinf,* **2005**, *58* (2), 278–284.

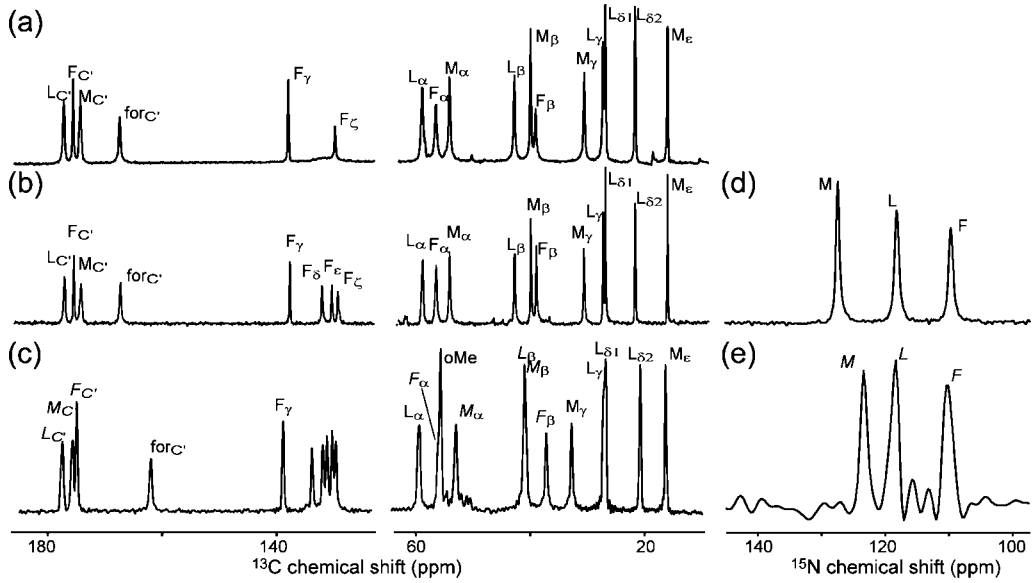

Figure 2. Assignment of one-dimensional ^{13}C and ^{15}N MAS spectra of N-*f*-MLF-OH and N-*f*-MLF-OMe recorded at room temperature: (a) ^{13}C spectra of natural abundance N-*f*-MLF-OH; (b) unlabeled N-*f*-MLF-OH with a ^{2}H-labeled Phe side chain (Phe-d_5); (c) natural abundance N-*f*-MLF-OMe; (d) ^{15}N spectrum of N-*f*-[U$-^{13}$C,^{15}N]MLF-OH; (e) natural abundance ^{15}N spectrum of N-*f*-MLF-OMe. Assignments for N-*f*-MLF-OMe were made in analogy with N-*f*-MLF-OH, with ambiguities denoted with italicized labels.

TURBOPOWDER[64] in order to determine the mechanism and rate of the Phe ring motion. The spectra from the δ and ε ^{2}H's were simulated separately from those of the terminal ζ deuteron and the resulting spectra combined, allowing line shape and intensity to be matched to the experimental variable-temperature data.

Structural Measurements. Details concerning the MAS SSNMR pulse sequences used for structural measurements are included in the Supporting Information. ^{15}N$-^{13}$C distances were measured using the 3D TEDOR pulse sequence.[43] The data were fit using an approximate analytical model of the spin dynamics for multiple, coupled spins under TEDOR[43] using a Levenberg$-$Marquardt algorithm for minimization of the χ^2 fit parameter.

Backbone torsion angle measurements were performed using HNCH and HN$_{i+1}$C$_i$H tensor correlation experiments.[44,52] The correlated dephasing under ^{1}H$-^{15}$N and ^{1}H$-^{13}$C couplings is monitored through the intensity of the ^{15}N$-^{13}$C cross peaks as a function of the synchronously incremented dipolar mixing time. The relative rate of incrementation was chosen to optimize the sensitivity of the experiment (in this case, $n = 2$). In these experiments, TMREV-4 was applied at a spinning frequency of 8.333 kHz.[65] The 3D HCCH experiment[66] for side chain torsion angle measurements was implemented as shown in the Supporting Information. Double quantum coherence, generated with band selective homonuclear recoupling sequence SPC5$_3$, dephases under the recoupled ^{1}H$-^{13}$C dipolar interactions and can be used to constrain the χ angle.[67] In the related NCCN experiment,[46,51,68] which provides constraints on the Ψ backbone torsion angle, SPC5$_3$ was used to generate double quantum coherence between C$'-$Cα. Here, REDOR[42] is used to simultaneously recouple the N$-$C$'$ and N$-$Cα interactions, causing Ψ-dependent dephasing of the DQ coherence. In a future publication, we plan to describe a detailed structural study of both forms of the N-*f*-MLF-OH peptide described here.

Results

Room-Temperature Measurements. Figure 2 shows the 1D solid-state MAS NMR spectra at room temperature for both N-*f*-MLF-OH and N-*f*-MLF-OMe. In N-*f*-MLF-OMe, the chemical shifts of each ^{13}C in the phenyl ring of N-*f*-MLF-OMe are distinct, indicating a static structure without dynamics on the NMR time scale. The ring in the N-*f*-MLF-OH peptide, on the other hand, is undergoing 180-degree flips, averaging the chemical shifts of Cδ and Cε ring ^{13}C's. Because of interference of the ring dynamics with the heteronuclear ^{1}H$-^{13}$C decoupling,[37,38] these carbon signals are broadened, unless the Phe side chain is deuterated (compare panels (a) and (b)), thus eliminating the strong heteronuclear (^{1}H$-^{13}$C) and homonuclear (^{1}H$-^1$H) dipolar couplings.

Temperature Dependence. Both peptides were examined by ^{13}C and ^{15}N magic angle spinning NMR over the temperature range 90$-$300 K and the spectra revealed remarkable differences in behavior. This is most obvious in the 1D ^{15}N spectra illustrated in Figure 3, where on cooling natural abundance N-*f*-MLF-OMe from 300 to 90 K the spectra do not change significantly. Because the ^{15}N chemical shift is a sensitive indicator of structure and dynamics, it appears that there is little change in either property. In contrast, the ^{15}N spectra of the (isotopically labeled) N-*f*-MLF-OH analog show a significantly different pattern (Figure 3b). Upon cooling below 200 K, a second set of lines appears and coexists with the original peaks (observed at room temperature), but diminishes again in intensity as the sample is further cooled to 90 K or below. As illustrated in Figure 3c, spectra acquired when the sample is warmed from 90 to 243 K reveal a significant hysteresis in the relative intensities of the lines from the two coexisting forms.

The temperature-dependent behavior was also examined using ^{13}C MAS NMR. As shown in Figure 4, there are no changes in the ^{13}C chemical shifts for the N-*f*-MLF-OMe ^{13}C sites as a

(63) Davis, J. H.; Jeffrey, K. R.; Bloom, M.; Valic, M. I.; Higgs, T. P. *Chem. Phys. Lett.* **1976**, *42*, 390–394.
(64) Wittebort, R. J.; Olejniczak, E. T.; Griffin, R. G. *J. Chem. Phys.* **1987**, *86* (10), 5411–5420.
(65) Hohwy, M.; Jaroniec, C. P.; Reif, B.; Rienstra, C. M.; Griffin, R. G. *J. Am. Chem. Soc.* **2000**, *122* (13), 3218–3219.
(66) Feng, X.; Verdegem, P.; Lee, Y.; Sandstrom, D.; Eden, M.; Bovee-Geurts, P.; de Grip, W.; Lugtenburg, J.; de Groot, H.; Levitt, M. *J. Am. Chem. Soc.* **1997**, *119* (29), 6853–6857.
(67) Hohwy, M.; Rienstra, C. M.; Griffin, R. G. *J. Chem. Phys.* **2002**, *117* (10), 4973–4987.
(68) Costa, P. R.; Gross, J. D.; Hong, M.; Griffin, R. G. *Chem. Phys. Lett.* **1997**, *280*, 95–103.

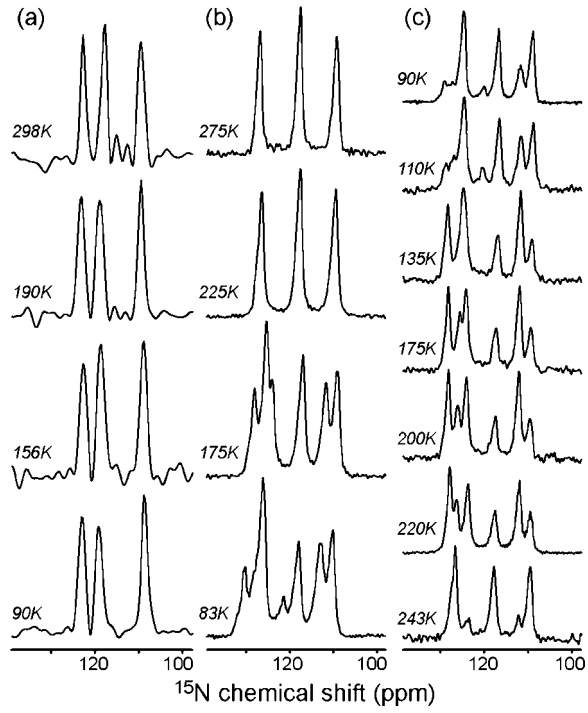

Figure 3. Variable-temperature ^{15}N spectra of (a) natural abundance N-*f*-MLF-OMe and (b, c) 10% N-*f*-[U−^{13}C,U−^{15}N]-MLF-OH. (a) No spectral changes are observed when cooling unlabeled N-*f*-MLF-OMe. (b) Cooling N-*f*-MLF-OH below 200 K yields spectra with extra lines. (c) Spectra obtained upon warming N-*f*-MLF-OH from 90 K to room temperature illustrating the hysteresis in the phase transition.

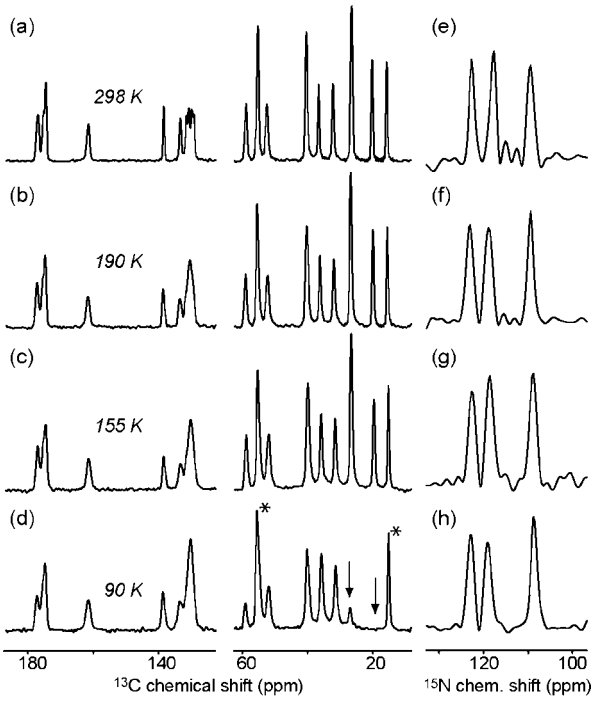

Figure 4. Variable-temperature 1D spectra of unlabeled N-*f*-MLF-OMe. (a−d) ^{13}C and (e−h) ^{15}N spectra recorded at 298, 190, 155, and 95 K. Data were acquired at $\omega_r/2\pi = 6.25$ kHz. Arrows indicate Leu methyl resonances that are most strongly attenuated at low temperature. Less restricted methyl resonances, indicated with "*", remain unaffected.

function of temperature. However, we do observe significant changes in line widths and intensities for several lines. The most dramatic perturbations are to the resonances corresponding to the two methyl groups of the Leu side chain (indicated with arrows in the Figure 4d). The observed intensity loss is due to the fact that the rate of 3-fold motion of the $-CH_3$'s becomes comparable to the decoupling field.[37,38] Note that other methyl groups in the Met side chain and the −OMe at the C-terminus (marked with "*" in Figure 4) experience less steric hindrance and thus do not exhibit these intensity losses.

In the case of the Leu and Met methyl groups of N-*f*-MLF-OH, we observed similar behavior, with significant intensity losses in the Leu methyl resonances, and less effect on the Met methyl resonance. However, as illustrated in Figure 5 with ^{13}C spectra of the natural abundance peptide, we now also observe substantial changes in the number of observed signals and their apparent line widths when cooling below 200 K, coinciding with the appearance of the additional signals in the ^{15}N spectra of N-*f*-MLF-OH (Figure 3). In particular, as shown in Figure 5b, we observe the formation of an additional, distinct spectroscopic "form" of the peptide between 200 and 90 K. Note also that at 200 K and below, the resonances of the Phe aromatic ring increase in intensity, and at 90 K, additional individual peaks are visible, indicating that the 180° ring flipping has ceased. Finally, we observe that the resolution in the spectrum is largely restored at 90 K, as illustrated in Figure 5a (bottom), and that most resonances exhibit ^{13}C chemical shifts similar to the values at room temperature.

Assignment Experiments. We performed two-dimensional chemical shift correlation experiments to generate site-specific assignments at 298, 175, and 90 K. The results of these measurements are summarized in Figures 6−8. Figure 6 shows the 2D ^{13}C−^{13}C correlation spectra recorded at each temperature. These spectra alone provide complete ^{13}C assignments of all resonances, with the exception of those that disappear upon cooling (e.g., various methyl signals). We observe a single form of the peptide at 298 and 90 K, but a mixture of two forms at 175 K. Of these, one "persistent" form has chemical shifts that resemble those of the room temperature and 90 K forms of N-*f*-MLF-OH, while the other form is a novel, "transitional", form that arises as the sample approaches a temperature of 175 K. Figure 7 highlights the aliphatic Cα−Cβ region, where the correspondence in chemical shift is most apparent. It is easy to see from these spectra that the cross-peak widths in the 175 K spectrum are essentially identical to those observed at 298 and 90 K. Therefore, we conclude that the apparent loss of resolution in the 1D spectra, for instance in the Cα region near 50−60 ppm, is caused by the emergence of this second structural form at intermediate temperatures rather than by line broadening due to conformational disorder. Heteronuclear correlation spectroscopy measurements served to provide sequential assignments, thereby assigning the ^{15}N chemical shifts and confirming our ^{13}C assignments. The NCACX and NCO spectra at 175 K are shown in Figure 8, along with their cross peak assignments. Based on these assignments, we could assign the extensive variable temperature 1D data (see for example Figures 2−4), track the change in chemical shift as a function of temperature, and monitor the appearance of the transitional form below 200 K. Tables containing the chemical shifts and assignments are available as Supporting Information.

(69) Takegoshi, K.; Nakamura, S.; Terao, T. *Chem. Phys. Lett.* **2001**, *344* (5−6), 631–637.
(70) Takegoshi, K.; Nakamura, S.; Terao, T. *J. Chem. Phys.* **2003**, *118*, 2325–2341.
(71) Morcombe, C. R.; Gaponenko, V.; Byrd, R. A.; Zilm, K. W. *J. Am. Chem. Soc.* **2004**, *126*, 7196–7197.

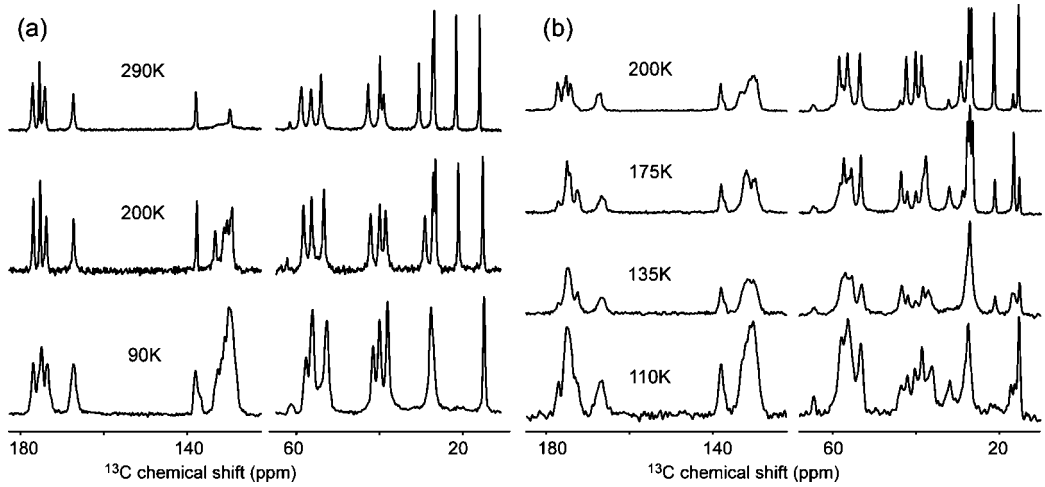

Figure 5. Variable-temperature 1D spectra of unlabeled N-*f*-MLF-OH. Column (a) shows the coarse temperature dependence between 290 and 90 K. (b) Spectra illustrating the spectral changes and apparent linebroadening associated with the transition between 200 and 110 K.

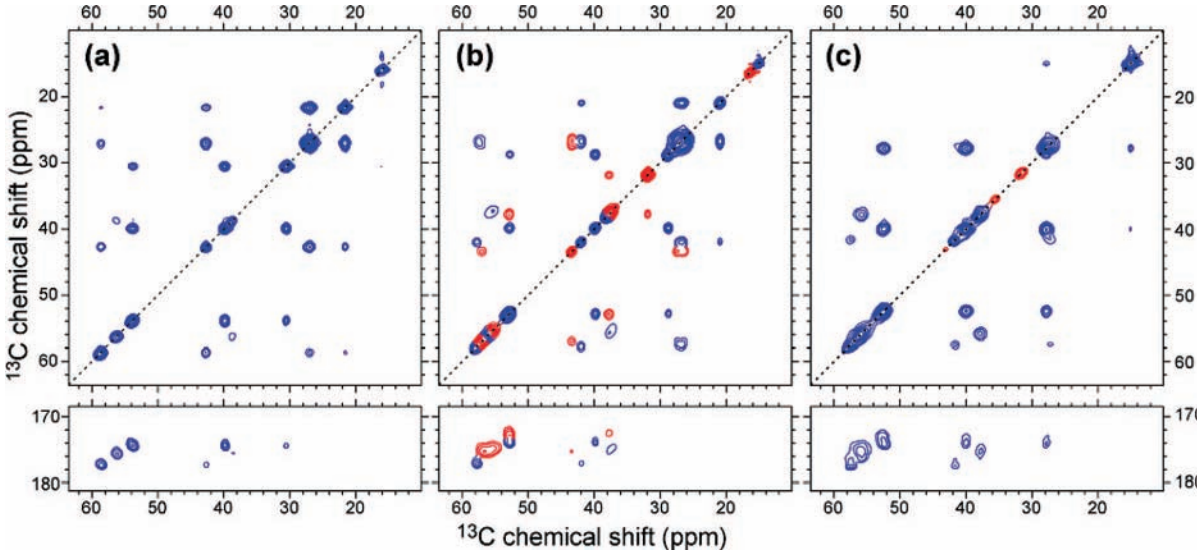

Figure 6. ^{13}C−^{13}C correlation spectra of 10% N-*f*-[U−^{13}C,U−^{15}N]-MLF-OH at (a) 298, (b) 175, and (c) 90 K. A DARR[69−71] mixing time of 10 ms resulted in single bond and weaker two-bond correlations. The top and bottom panels show aliphatic−aliphatic and carbonyl−aliphatic cross-peaks, respectively. For clarity, cross-peaks from the novel "transitional" form seen at 175 K are highlighted in red.

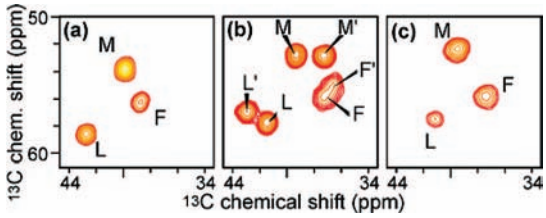

Figure 7. Expanded regions from the experimental spectra shown in Figure 6, highlighting the ^{13}Cα−^{13}Cβ cross-peaks, at (a) 298, (b) 175, and (c) 90 K. Assignments for the novel transitional form are marked with a prime (e.g., M′ vs M).

Characterization of the Dynamics. The difference in behavior between the two peptides, namely the presence or absence of a transitional form, appears to correlate with differences in their dynamics. For both peptides, we observe the expected 3-fold hopping motion of the methyl groups, with a loss of intensity in the Leu methyl groups at reduced temperatures. Further, in N-*f*-MLF-OH, we observed evidence of Phe ring motion, which is absent in N-*f*-MLF-OMe. Therefore, we also examined the molecular dynamics through a number of solid state MAS experiments. The ^{1}H−^{13}C dipolar interaction is attenuated by any dynamics and was therefore measured using the TMREV recoupling sequence.[65] The ^{1}H−^{13}C dipolar couplings of several ^{13}C−^{1}H groups change significantly as a function of temperature (see the Supporting Information). At room temperature, the methyl dipolar couplings are averaged due to a 3-fold hopping motion, and, as the temperature is reduced, the methyl motions slow and their C−H dipolar couplings increase until they reach a limit near 200−225 K. The temperature-dependence for the magnitude of the scaled dipolar coupling is also found to be residue dependent, consistent with the observations in the 1D ^{13}C spectra. There is also a large change in the behavior of the aromatic carbon sites, which are mobile down to 250 K but progressively slow down as the temperature approaches 165 K.

The motion of the phenyl ring was examined in more detail with ^{2}H NMR quadrupole echo experiments on crystals of N-*f*-MLF-OH containing a deuterated phenyl ring (Phe-d_5). Figure 9a shows the resulting ^{2}H 1D powder spectra at a number of temperatures. Fits of the powder line shape (panel b) and of the quadrupolar echo intensity data (panels c and d) indicate

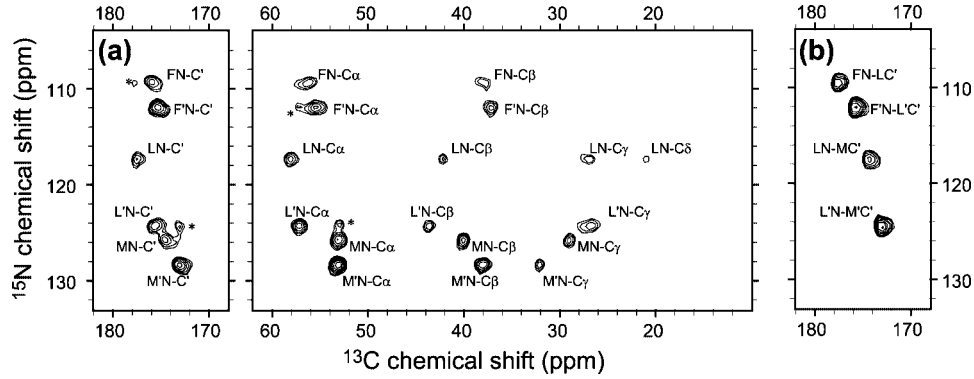

Figure 8. 2D $^{15}N-^{13}C$ correlation spectra on [10% U$-^{13}C,^{15}N$ N-*f*-MLF-OH] at 175K and 8 kHz MAS: (a) NCACX, with 10 ms DARR $^{13}C-^{13}C$ mixing, showing intraresidue assignments (asterisks mark several weak inter-residue correlations); (b) NCO 2D showing sequential N$-$C′ cross-peak assignments. Assignments for the novel transitional form are marked with a prime (e.g., M′ vs M).

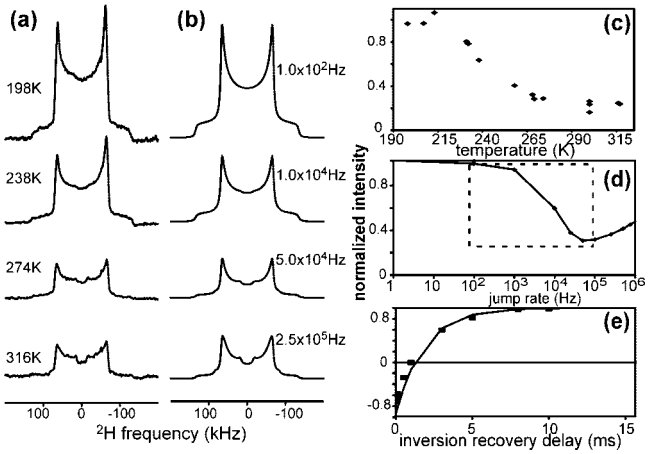

Figure 9. Static deuterium NMR data for N-*f*-ML[F-d_5]-OH. (a) 1D spectra (left) at 198$-$316 K together with (b) simulated spectra for estimated Phe flipping rates, (c) overall signal intensity of observed signal at 198$-$316 K, (d) simulated flipping rate dependence of signal intensity for Phe-d_5, with the dashed box indicating the range of conditions matching the experimental results, and (e) room temperature inversion recovery measurement with simulated curve at 3.5×10^5 Hz flipping rate.

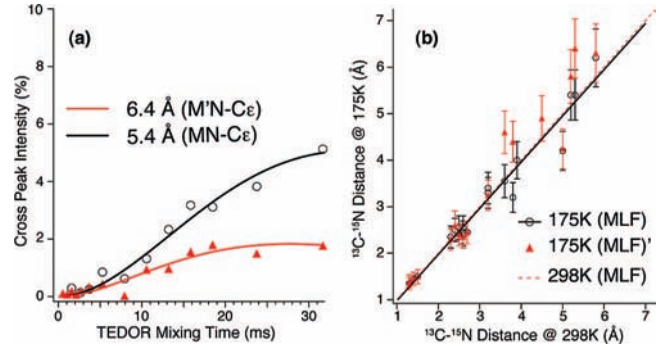

Figure 10. (a) Example of fitting (solid lines) of long distances in TEDOR experiments, showing the Met N$-$Cε distance at 175K. Experimental data are shown as open circles (persistent form) and solid triangles (transitional form). (b) Comparison of 175 and 298 K N$-$C distances. The transitional form (MLF)′ has systematically longer distances than the persistent form (MLF), which closely resembles the room temperature structure. The solid and dashed lines indicate the linear correspondence for the room temperature and "persistent" form at 175 K.

that the ring is executing 180° flips at a rate that varies from $<1 \times 10^2$ s^{-1} near 200 K to $\sim 1 \times 10^5$ s^{-1} near room temperature. The latter was confirmed with room-temperature inversion recovery measurements (shown in panel e). An Arrhenius analysis of the estimated hopping rates reveals an activation energy for ring flip of ~38 kJ/mol, which is similar to the activation energies observed for a number of other crystalline Tyr- or Phe-containing peptides.[72,73]

Structural Measurements. To examine the structural features of the two forms of N-*f*-MLF-OH that coexist at 175 K, we used dipolar recoupling experiments to measure heteronuclear $^{13}C-^{15}N$ distances [34,42,43] and tensor correlation experiments [33,44−52] to constrain backbone and side chain torsion angles. All measurements were conducted using a sample consisting of uniformly $^{13}C,^{15}N$-labeled N-*f*-MLF-OH diluted to 10% in natural abundance peptide prior to crystallization, to minimize the effects of intermolecular dipolar couplings. Distance constraints were obtained via 3D TEDOR[43] experiments performed at 298, 175, and 90 K. This resulted in numerous intramolecular $^{13}C-^{15}N$ distances, which are tabulated in the Supporting Information. An example of the fit for weak dipolar couplings corresponding to distances of 5.4 and 6.4 Å (Met$-$N-Cε) is shown in Figure 10a. Note that the approximate analytical model used to fit these data neglects the orientation dependence of the spin dynamics and hence introduces a systematic error of approximately 10$-$20%, which is greater than the random error in these data.

These $^{15}N-^{13}C$ distances allow initial structural comparisons of the coexisting 175 K forms and provide insights into the localization of the largest changes. Figure 10b shows a comparison of both forms to the room temperature structure, indicating that the persistent form is structurally similar to the room temperature form. The transitional structure is characterized by an overall increase in the measured $^{13}C-^{15}N$ distances (see also Figure S2 in the Supporting Information). Although the distances in the persistent structure vary at most 8% (or 0.4 Å) from the equivalent distance at 298 K, the transitional structure displays much larger changes of as much as 45% (or 1.3 Å).

To obtain further structural information, side chain and backbone torsion angle were measured using a number of techniques. These experiments incorporate the TMREV sequence for γ-encoded heteronuclear recoupling of the $^1H-^{13}C$ dipolar coupling[65] or REDOR for recoupling of the $^{15}N-^{13}C$ dipolar interaction.[42] A 3D HCCH experiment allowed the

(72) Rice, D. M.; Meinwald, Y. C.; Scheraga, H. A.; Griffin, R. G. *J. Am. Chem. Soc.* **1987**, *109* (6), 1636–1640.
(73) Kamihira, M.; Naito, A.; Tuzi, S.; Saito, H. *J. Phys. Chem. A* **1999**, *103* (18), 3356–3363.

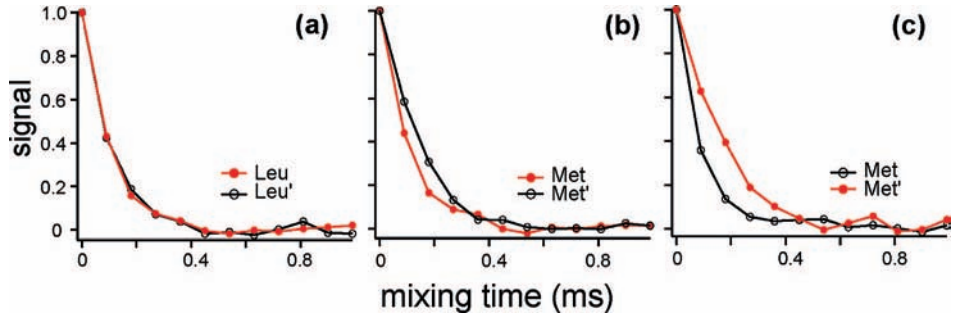

Figure 11. Experimental data from HCCH tensor correlation experiment designed to measure N-*f*-MLF-OH side chain torsion angles at 175 K: (a) Leu χ_1, (b) Met χ_1, and (c) Met χ_2. The results show that the Met side chain conformation is different between the two forms of MLF, which coexist at 175 K.

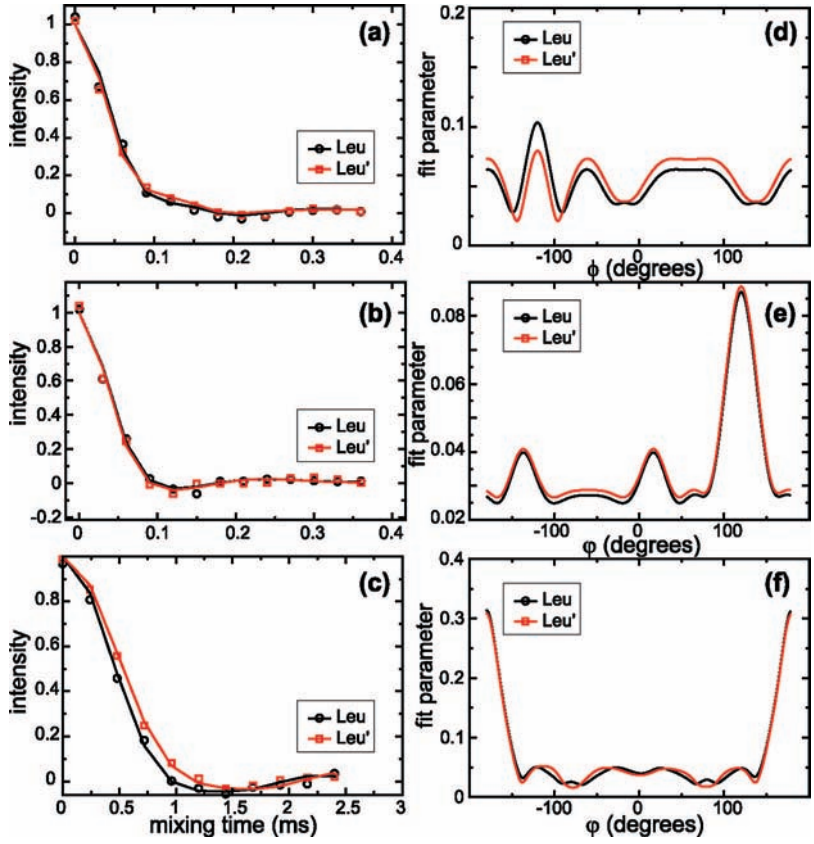

Figure 12. Examples of data fitting and resulting solution surfaces for the backbone torsion angles of Leu in both forms at 175 K. Measurements involved (a, d) ϕ measured via HNCH, (b, e) ψ via $HN_{i+1}C_iH$, and (c, f) NCCN tensor correlation experiments.

simultaneous examination of multiple side chain torsion angles in the coexisting N-*f*-MLF-OH forms found at 175 K. The measurement resulted in dephasing trajectories (Figure 11) suggesting very similar Leu side chain conformations, but a significant conformational difference in the Met side chain. The backbone ϕ and ψ torsion angles were accurately constrained through HNCH and $HN_{i+1}C_iH$ experiments, with secondary constraints on ψ through NCCN dipolar correlation experiments. Representative data for the Leu residue are shown in Figure 12 (additional data are in the Supporting Information). The figure also includes simulated fit curves obtained in the analysis of these torsion angle data. These fit results illustrate the complementary angular sensitivity for the various backbone torsion angle techniques. Solutions for the torsion angle are inherently dependent on the precise value of the heteronuclear $^1H-^{15}N$ and $^1H-^{13}C$ couplings and on the three-atom bond angles used in the calculation of the projection angles. For all fits, we used the equilibrium parameters specified in the X-Plor NIH[74] NMR refinement force-field for consistency. The expected variation of bond angles about these average values can induce a $\pm 10-15°$ uncertainty in the solution for the projection angle, which in all cases exceeds the random error in these experiments. The calculated torsion angles are included as Supporting Information and indicate that the backbone conformation is similar between the two structural forms.

Discussion

We have obtained detailed experimental data on the dynamic and structural behavior of two microcrystalline tripeptides as a function of temperature. These polypeptide lattices are devoid of water or organic solvent molecules (tested explicitly via Karl

(74) Schwieters, C. D.; Clore, G. M. *J. Magn. Reson.* **2001**, *152* (2), 288–302.

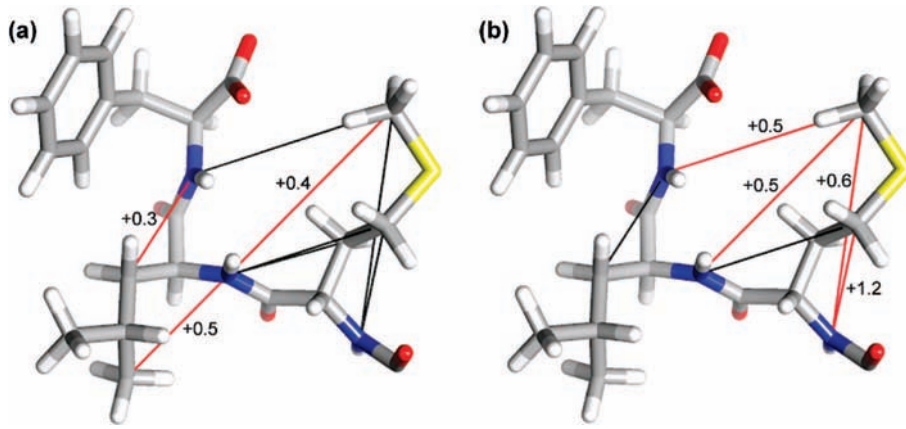

Figure 13. Illustration of the deviation from the room temperature distances[34,36] for each of the measured $^{15}N-^{13}C$ measurements at 175 K, for (a) the persistent form (MLF) and (b) the transitional form (MLF)′. Each of the observed distances is indicated by a line, with those that deviate by more than 0.25 Å highlighted and marked with the deviation (in Å). The largest deviations are located in the Met side chain. This figure was prepared using UCSF Chimera.[75]

Fischer water analysis at Galbraith Laboratories, Inc., Knoxville, TN; results not shown) and therefore all observations reflect intrinsic polypeptide dynamics. Consistent with the absence of solvent and established features of dehydrated protein dynamics, there was no evidence of a dynamic or structural transition between 200 and 240 K. As discussed in the introduction, this is the typical regime where the solvent-dependent protein glass transition takes place. However, our NMR data do show a structural transition specific to one of the peptides at temperatures between 90 and 200 K. This appears to reflect a distinct difference in motional behavior between the two tripeptide crystal lattices, despite their similar chemical structure and crystallization behavior. Specifically, the O-methylated peptide N-*f*-MLF-OMe forms a largely rigid system and temperature-dependent changes in its NMR spectra are relatively small and confined to 3-fold hopping of the methyl groups which is manifest in large changes in their ^{13}C signal intensities with temperature. We further noted significant variations in methyl group dynamics between different residues that are correlated to the extent of steric hindrance to the methyl group 3-fold jump. The motional interference with the $^{1}H-^{13}C$ decoupling[37,38] due to a reduction in CH_3 jump rate occurs at a higher temperature for the Leu side chain methyls than for the Met CH_3 group, which remains mobile down to 90 K, preventing such destructive interference. The ^{15}N and ^{13}C resonance chemical shifts are basically temperature independent in N-*f*-MLF-OMe, including those of the Phe side chain (which is immobile even at room temperature).

Spectra of the N-*f*-MLF-OH peptide reveal similar methyl group dynamics (disappearance of Leu methyls). Additional measurements of the CH_3 motions based on the reduction in the $^{13}C-^{1}H$ dipolar coupling reinforce the observation of residue-type dependence, with substantial modulation of the temperature-dependence due to differences in the steric environment. Unlike the O-methylated peptide, there are significant additional structural and dynamical changes upon cooling. These effects include the temperature-correlated emergence of a second conformational substate that arises below 200 K and then eventually disappears upon cooling to 90 K. We applied several solid-state NMR methods to measure structural parameters of the peptide at 175 K, where this "transitional" form coexists with a "persistent" form that is present at both room temperature and 90 K.

The measured distance and backbone torsion angle data (tabulated in the Supporting Information) were used for structure refinement, employing protocols for simulated annealing molecular dynamics[41] as implemented in the program X-Plor-NIH.[74] Because of the absence of side chain constraints at 90 K, no structural refinement was attempted for N-*f*-MLF-OH at this temperature. In addition, conformational ensembles obtained from refinement at 175 K are presently of insufficiently high resolution to allow a detailed structural analysis. Thus, we are continuing these experiments and will report them in a future publication. Nevertheless, we can draw some conclusions about the structural changes during the dynamically driven transition. The backbone structure was found to be preserved (as indicated by the backbone torsion angle measurements). The experimental data indicate changes in the conformation of the side chains, in particular the Met side chain. This is apparent from the torsion angle measurements (Figure 11), where a significant change is observed in the Met χ_2 angle. Similar conclusions can be drawn from the distance measurements, as illustrated in Figure 13. This figure shows the room temperature SSNMR structure of N-*f*-MLF-OH[36] with lines indicating the measured internuclear distances. The distances that deviate from their room temperature values are highlighted in color, alongside the change in distance in angstroms. Also here, a large consistent change is occurring in the Met side chain. In addition, we observed a significant increase in the Leu $N-C\gamma/C\delta1$ distance (due to overlap, the carbon sites could not be distinguished), suggesting that the Leu side chain is oriented differently in the transitional form. Because the Leu χ_1 angle was found to be the same between the two forms (Figure 11), the difference must be due to a change in the Leu χ_2 angle (analogous to Met).

Let us now compare N-*f*-MLF-OH with N-*f*-MLF-OMe and their behaviors upon cooling. The room-temperature monomer structure of N-*f*-MLF-OH was previously determined by solid-state NMR[36] and was found to resemble the X-ray structure of N-*f*-MLF-OMe.[30] Further, X-ray powder diffraction data suggest that the unit cell and space group of both peptide crystals are similar (see the Supporting Information). These structural similarities indicate that the spectral differences are due to differences in the dynamics and that the transition represents a

(75) Pettersen, E. F.; Goddard, T. D.; Huang, C. C.; Couch, G. S.; Greenblatt, D. M.; Meng, E. C.; Ferrin, T. E. *J. Comput. Chem.* **2004**, *25* (13), 1605–1612.

low-temperature dynamic transition, correlated to a structural transition (i.e., one that does not occur in the absence of these dynamics). In the conventional picture of temperature-activated conformational exchange as monitored by NMR, a transition between two states results in spectra with an averaged, narrow resonance at high temperature, a broad, single resonance at intermediate temperatures, and separate narrow resonances at temperatures low enough to arrest the dynamics. Interestingly, N-*f*-MLF-OH does not display this behavior, but rather shows a distribution between two distinct, similarly narrow sets of NMR lines at intermediate temperatures. Even more atypical seems the observation that the form that appears upon cooling subsequently disappears at even lower temperatures.

Indeed, the phase transition in N-*f*-MLF-OH takes place between 200 and 100K where, concomitantly, there is a drastic reduction in the intensity of the methyl group resonances. The observed dynamic event does correlate with the observed onset of anharmonic motion at temperatures above 100K, which was proposed to be associated with methyl group motion.[12,16,26,76] However, our system highlights the fact that another potentially important source of mobility in proteins is the aromatic side chains, such as phenylalanine. Specifically, the methyl dynamics are present in N-*f*-MLF-OMe as well and therefore do not account for the observed transition. In fact, the most visible difference between the N-*f*-MLF-OH and N-*f*-MLF-OMe crystals is in the rate of reorientation of the Phe ring. As illustrated in Figure 1, the aromatic ring in N-*f*-MLF-OMe is prevented from flipping by the close proximity of a number of bulky groups, including the C-terminal methyl group (OMe). In contrast, the ^{13}C and ^{2}H spectra clearly show that the Phe ring in N-*f*-MLF-OH is executing 180° flips. This suggests that the observed transition may be correlated directly to a change in the motion of the aromatic phenyl ring. Qualitatively, the fact that a methyl group was removed, whereas the unit cell remains (virtually) the same, seems consistent with the increased mobility of the phenyl ring (the unit cell is actually slightly larger for N-*f*-MLF-OH). The measured temperature dependence of the Phe ring flips (based on the static ^{2}H measurements) indicates a drastic reduction of the flipping rate from $\sim 1 \times 10^5$ s^{-1} near room temperature to <100 s^{-1} when the temperature drops below 190 K. In this regime of slow motion, it is conceivable that the ring can become kinetically trapped in an intermediate orientation. Because of packing interactions in the lattice, the ring flip can be accommodated through concerted motions of surrounding side chains, resulting in the long-range conformational changes evidenced, in turn, by changes in the chemical shift and quantitative structural and dynamical solid state NMR measurements. Changes in the proximity and orientation of the phenyl ring can also directly (and substantially) change the chemical shifts of surrounding nuclei through ring current effects.[77] This complicates the interpretation of chemical shift changes in terms of local structural changes, and highlights the importance of explicit quantification of distances, torsion angles and dynamics (as shown here). The structural measurements show that the predominant structural changes are in the χ_2 side chain torsion angles of the Met and Leu residues, which are close to the Phe ring (see Figure 1) and thus could correlate to its change in dynamics.

Because no intermediate rate exchange dynamics are observed, it appears that our measurements elucidate the end points of the structural and dynamic transition but might not provide direct information on its mechanism. It is reasonable to ask whether or not the activation of these dynamical modes is necessary for the structural phase transition to occur, or if the reverse is true. Further, the experiments presented here do not directly probe the degree to which motion or transient reorganization of the lattice itself is coupled to the dynamics.[78,79] Both questions might be probed by molecular dynamics simulations of many unit cells of the N-*f*-MLF-OH lattice. The latter issue can be studied in isolation using NMR samples that are prepared to yield exclusively intermolecular couplings (e.g., 50% ^{15}N-N-*f*-MLF-OH in 50% ^{13}C-N-*f*-MLF-OH), or by approaches based on $^{1}H-^{1}H$ spin diffusion.[80] Further studies may also prove important for the accurate estimation of dipolar couplings and torsion angles in the presence of dynamics,[81] a condition that is likely to occur in a physiological environment.

Protein Dynamics and Applications at Low Temperature. The tripeptide N-*f*-MLF-OH is a model system that experiences a subset of the structural dynamics experienced by proteins. Although methyl dynamics have been invoked to explain the glass transition in the past,[13] one increasingly distinguishes the canonical protein glass transition dominated by coupling to the solvent from distinct contributions due to intrinsic polypeptide dynamics. A complete understanding of these low-temperature transitions is limited by a lack of site-resolved experimental data on the structure and motions involved. We have shown that low temperature MAS SSNMR can provide site specific insights into the molecular nature of low temperature dynamics in peptides and proteins. In general, low-temperature applications of solid state NMR include not only conventional NMR on microcrystalline model proteins,[82,83] but also dynamic nuclear polarization experiments in membrane proteins and other systems.[39,84,85] Examining the source of line broadening sometimes reported at reduced temperatures is therefore also of practical interest. We observe here that line broadening as a result of cooling to low temperatures (even in a dynamic system) does not preclude low-temperature NMR experiments, but that apparent line broadening in these spectra reflects discrete forms of the peptide that are resolved in spectra of higher dimensionality. Remarkably, we actually observe a reduction in this multiplicity at even lower temperatures (near 90 K). It will be of interest to examine whether this type of behavior is unique to this system, or can also be observed in other peptides as well as in hydrated proteins, where solvent-dependent mechanisms may result in broadening of NMR lines near the protein glass transition. Indeed, the observation that temperature-induced line broadening is reversible in microcrystalline systems tends to exclude cold-denaturation or damage to the crystalline lattice

(76) Cottone, G.; Giuffrida, S.; Ciccotti, G.; Cordone, L. *Proteins: Struct., Funct., Bioinf.* **2005**, *59* (2), 291–302.
(77) Ma, Z.; Halling, M. D.; Solum, M. S.; Harper, J. K.; Orendt, A. M.; Facelli, J. C.; Pugmire, R. J.; Grant, D. M.; Amick, A. W.; Scott, L. T. *J. Phys. Chem. A* **2007**, *111* (10), 2020–2027.
(78) Pschorn, U.; Rossler, E.; Sillescu, H.; Kaufmann, S.; Schaefer, D.; Spiess, H. W. *Macromolecules* **1991**, *24* (2), 398–402.
(79) Schaefer, J.; Sefcik, M. D.; Stejskal, E. O.; Mckay, R. A.; Dixon, W. T.; Cais, R. E. *Macromolecules* **1984**, *17* (6), 1107–1118.
(80) Elena, B.; Pintacuda, G.; Mifsud, N.; Emsley, L. *J. Am. Chem. Soc.* **2006**, *128* (29), 9555–9560.
(81) Lorieau, J. L.; McDermott, A. E. *J. Am. Chem. Soc.* **2006**, *128* (35), 11505–11512.
(82) Martin, R. W.; Zilm, K. W. *J. Magn. Reson.* **2003**, *164*, 162–174.
(83) Franks, W. T.; Zhou, D. H.; Wylie, B. J.; Money, B. G.; Graesser, D. T.; Frericks, H. L.; Sahota, G.; Rienstra, C. M. *J. Am. Chem. Soc.* **2005**, *127*, 12291.
(84) Hall, D. A.; Maus, D. C.; Gerfen, G. J.; Inati, S. J.; Becerra, L. R.; Dahlquist, F. W.; Griffin, R. G. *Science* **1997**, *276* (5314), 930–932.
(85) van der Wel, P. C. A.; Hu, K.-N.; Lewandowski, J. R.; Griffin, R. G. *J. Am. Chem. Soc.* **2006**, *128*, 10840–10846.

by freezing as a source of this broadening.[82,83] Line broadening and intensity losses can also result from motional interference with heteronuclear $^{1}H-^{13}C$ and $^{1}H-^{15}N$ decoupling,[37,38] as is observed for the Phe ring in N-*f*-MLF-OH at room temperature and methyl groups at reduced temperatures. Figure 2 shows that deuteration of side chains can serve as one approach to circumvent this problem. In a complicated system such as a hydrated protein, we expect many such mechanisms to contribute to the observed behavior at low temperatures. In our solvent-free system, we can show that the dynamics of the aromatic ring appear correlated with temperature-driven structural transitions in this peptide. In general, our results suggest that solid-state NMR can make an important contribution to studies of low temperature dynamics of proteins. This can extend to larger protein systems, but because of the complexities involved, we feel that simulations and measurements on model systems such as the one described here will prove essential for a thorough biophysical understanding. Experimental insights such as those presented here can serve as checks of, and input for, detailed computational analyses. We intend to obtain further structural and dynamical data on the peptide crystal lattices discussed here in ongoing solid state NMR studies.

Acknowledgment. We thank Dr. Lisa Tucker-Kellogg for discussions and help with the structure calculations; Ajay Thakkar, Jeff Bryant, and Dr. David Ruben for valuable technical assistance; and Scott Speakman for performing the X-ray powder diffraction measurements. Figure 13 was produced using the UCSF Chimera package from the Resource for Biocomputing, Visualization, and Informatics at the University of California, San Francisco (supported by NIH P41 RR-01081). This work was supported by grants from the National Institutes of Health (EB-001960, EB-003151, and EB-002026). V.S.B. acknowledges the receipt of a PGS Fellowship from the Natural Sciences and Engineering Research Council of Canada.

Supporting Information Available: Schematic illustrations of employed pulse sequences, tables of chemical shifts and structural data obtained at various temperatures, crystal powder diffraction data, and figure showing the temperature-dependence of the $^{1}H-^{13}C$ dipolar couplings (PDF). This material is available free of charge via the Internet at http://pubs.acs.org.

JA8045926